Morphological instability during steady electrodeposition at overlimiting currents

Christoffer P. Nielsen and Henrik Bruus

Department of Physics, Technical University of Denmark,
*DTU Physics Building 309, DK-2800 Kongens Lyngby, Denmark**

(Dated: 27 May 2015, submitted to Phys. Rev. E)

We present a linear stability analysis of a planar metal electrode during steady electrodeposition. We extend the previous work of Sundstrom and Bark by accounting for the extended space-charge density, which develops at the cathode once the applied voltage exceeds a few thermal voltages. In accordance with Chazalviel's conjecture, the extended space-charge region is found to greatly affect the morphological stability of the electrode. To supplement the numerical solution of the stability problem, we have derived analytical expressions valid in limit of low and high voltage, respectively.

I. INTRODUCTION

One of the most interesting aspects of systems, involving transport between matter in different phases, is their tendency to become morphologically unstable and develop ramified growth patterns. Well known examples include snow flake formation and dendritic growth during metal solidification [1, 2]. A particularly interesting and challenging growth problem is encountered in electrodeposition from an electrolyte onto an electrode [3–11]. Whereas snow flake formation and solidification are mainly driven by diffusion of water vapour and heat, respectively [1, 2], electrodeposition is driven by electromigration in addition to diffusion [12, 13]. For this reason, the electrodeposition rate can be driven to exceed the diffusion limit, at which point the system enters a nonlinear regime not encountered in the purely diffusion-driven systems. One of the features of this nonlinear regime is the development of a nonequilibrium space-charge region, which extends from the cathode into the electrolyte [12, 14, 15]. Already in 1990, Chazalviel realized that this extended space-charge region is crucial to the understanding of ramified growth during electrodeposition [12]. Nevertheless, there has been very little work which actually takes this effect into account.

In this paper we investigate the morphological stability of the cathode during electrodeposition in both the linear and the nonlinear regime. We follow the approach of Sundstrom and Bark [16], and investigate steady electrodeposition in a system composed of an electrolyte sandwiched between two, initially planar, metal electrodes. We solve the stability problem numerically and find that the higher the applied voltage difference is, the more unstable the electrode surface becomes. Also, the most unstable wavelength becomes smaller as the voltage bias is increased.

In addition to solving the stability problem numerically, we derive analytical expressions for the perturbation growth rate, valid in the low and high voltage limit, respectively. In deriving these expressions, we make use
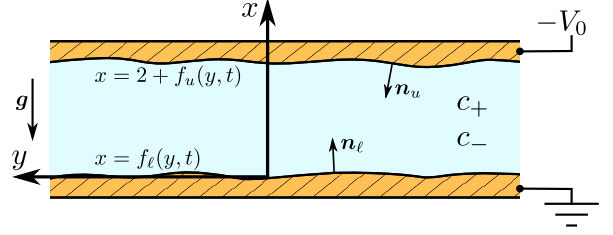
* chnie@fysik.dtu.dk and bruus@fysik.dtu.dk

FIG. 1. Sketch of the studied system with lower and upper electrode surfaces at $x = f_\ell(y,t)$ and $x = 2 + f_u(y,t)$, respectively. The coordinates are given relative to the moving frame of reference, following the mean speed of the electrode surfaces, and normalized by half the electrode spacing L.

of an accurate analytical model for the extended space-charge region, which we presented in a recent paper [15].

II. MODEL SYSTEM

Following Sundstrom and Bark [16], we consider a binary electrolyte trapped between two co-planar metal electrodes at $x = 0$ and $x = 2L$. The electrolyte has initial concentration c_0 and is assumed symmetric with valence Z. The coordinate system is moving in the negative x-direction with velocity U, which is related to the mean movement of the electrode. We consider the dilute solution limit, in which the effect of the moving coordinate system is negligible everywhere except in the surface evolution equation. A sketch of the system is shown in Fig. 1.

In the analysis, we investigate the stability of y-dependent perturbations along the x-direction. However, our analysis is general and applies to perturbations along any direction in the yz plane.

III. GOVERNING EQUATIONS

The current densities of either ion are given as

$$2\boldsymbol{J}_\pm = -c_\pm \boldsymbol{\nabla}\mu_\pm, \tag{1a}$$

$$\mu_\pm = \ln(c_\pm) \pm Z\phi, \tag{1b}$$

where we have non-dimensionalized the currents $\boldsymbol{J}_\pm$ by the limiting currents $2D_\pm c_0/L$, the electrochemical potentials $\mu_\pm$ by $k_B T$, the electric potential ϕ by the thermal voltage $V_T = k_B T/e$, the coordinates by half the electrode spacing L, and the concentrations $c_\pm$ by the initial concentration c_0. Normalizing the time by the diffusion time $t_0 = L^2/(2D_+)$, the non-dimensionalized ion-conservation equations become

$$\frac{D_+}{D_\pm}\partial_t c_\pm = -\boldsymbol{\nabla} \cdot \boldsymbol{J}_\pm. \tag{2}$$

At the electrodes, the current of anions vanishes, while the current of cations is given by a reaction expression

$$\boldsymbol{n}_p \cdot \boldsymbol{J}_- = 0, \tag{3a}$$
$$\boldsymbol{n}_p \cdot \boldsymbol{J}_+ = -R_p, \tag{3b}$$

where R_p is the reaction rate at the lower and upper electrode, respectively, as indicated by the subscript $p = \ell, u$. We model the reaction rates R_u and R_ℓ using the standard Butler-Volmer expression [16],

$$R_p = K_0 \left[c_+ e^{-\bar{\gamma}\kappa + \alpha Z(\phi+V_p)} - e^{-\bar{\gamma}\kappa - (1-\alpha)Z(\phi+V_p)} \right], \tag{4}$$

where K_0 is the dimensionless version of the dimensionfull rate constant k_0 for the electrode reaction,

$$K_0 = \frac{k_0}{2D_+ c_0/L}. \tag{5}$$

Above, V_p is the normalized electrode potential, κ is the normalized curvature of the surface, α is the charge-transfer coefficient, and $\bar{\gamma}$ is the non-dimensionalized version of the dimensionfull surface energy γ,

$$\bar{\gamma} = \frac{a^3 \gamma}{k_B T L}. \tag{6}$$

The electrostatic part of the problem is governed by the Poisson equation,

$$2\bar{\lambda}_D^2 \nabla^2 \phi = -\rho = -Z c_+ + Z c_-, \tag{7}$$

where the non-dimensional Debye length $\bar{\lambda}_D$ is given as

$$\bar{\lambda}_D = \frac{\lambda_D}{L}, \quad \text{with} \quad \lambda_D = \sqrt{\frac{k_B T \epsilon_w}{2e^2 c_0}}. \tag{8}$$

For simplicity, and to be in accordance with most previous work, we choose not to explicitly model the Debye layers adjoining the electrodes. Instead, we apply the boundary conditions (3) just outside the Debye layer. Following Ref. [17] we implement the boundary condition

$$\boldsymbol{n}_u \cdot \boldsymbol{\nabla} c_+ = 0, \tag{9}$$

at the upper electrode, to reflect the minimum in c_+ at the outer edge of the Debye layer. Together with

Eq. (3b), condition (9) corresponds to ascribing the entire current into the upper electrode to electromigration.

Finally, since the anions can not enter or leave the system the total number of anions is conserved,

$$\int_\Omega \left(c_- - 1 \right) \, \mathrm{d}V = 0. \tag{10}$$

We introduce functions $x = f_p(y)$ describing the position of the upper and lower electrode u and ℓ. The time evolution of f_p is determined by the single-ion volume a^3 and the current into the electrode,

$$(\partial_t f_\ell - U)\,\boldsymbol{e}_x \cdot \boldsymbol{n}_\ell = -a^3 c_0 \boldsymbol{n}_\ell \cdot \boldsymbol{J}_+, \quad \text{Anode}, \tag{11a}$$
$$(\partial_t f_u - U)\,\boldsymbol{e}_x \cdot \boldsymbol{n}_u = -a^3 c_0 \boldsymbol{n}_u \cdot \boldsymbol{J}_+, \quad \text{Cathode}. \tag{11b}$$

Here, the filling factor $a^3 c_0$ is much less than unity, since we are dealing with dilute solutions. The normalized velocity U of the coordinate system accounts for the mean current into or out off the electrodes, and $\partial_t f_p$ accounts for local deviations from the mean current.

The curvature κ and the normal vectors are related to the surface function f_p by

$$\boldsymbol{n}_\ell = \frac{\boldsymbol{e}_x - \boldsymbol{e}_y \partial_y f_\ell}{\sqrt{1 + (\partial_y f_\ell)^2}}, \quad \boldsymbol{n}_u = \frac{-\boldsymbol{e}_x + \boldsymbol{e}_y \partial_y f_u}{\sqrt{1 + (\partial_y f_u)^2}}, \tag{12a}$$

$$\kappa_\ell = \frac{\partial_y^2 f_\ell}{\sqrt{1 + (\partial_y f_\ell)^2}}, \quad \kappa_u = -\frac{\partial_y^2 f_u}{\sqrt{1 + (\partial_y f_u)^2}}. \tag{12b}$$

In defining the above equations and boundary conditions, we have chosen slightly different normalizations than in Ref. [16], the main difference being that we allow for a non-zero space charge density.

IV. PERTURBATION

The stability of the problem is investigated using linear perturbation theory. That is, we impose a small perturbation on a steady-state base state, and investigate how the perturbation evolves. The base state is identified by a superscript "0" and the first-order perturbation by superscript "1",

$$f_p(y,t) \approx f_p^1(y,t), \tag{13a}$$
$$c_\pm(x,y,t) \approx c_\pm^0(x) + c_\pm^1(x,y,t), \tag{13b}$$
$$\phi(x,y,t) \approx \phi^0(x) + \phi^1(x,y,t). \tag{13c}$$

In first-order perturbation theory, we substitute the second-order factor $\sqrt{1 + (\partial_y f_p)^2}$ in Eq. (12) by unity,

$$\boldsymbol{n}_\ell \approx \boldsymbol{e}_x - \boldsymbol{e}_y \partial_y f_\ell^1, \quad \boldsymbol{n}_u \approx -\boldsymbol{e}_x + \boldsymbol{e}_y \partial_y f_u^1, \tag{14a}$$
$$\kappa_\ell \approx \partial_y^2 f_\ell^1, \quad \kappa_u \approx -\partial_y^2 f_u^1. \tag{14b}$$

To find the field values at the perturbed surface, we Taylor expand to first order and obtain

$$\phi(f_\ell^1, y, t) \approx \phi^0(0) + \partial_x \phi|_0 f_\ell^1(y,t) + \phi^1(0,y,t), \tag{15a}$$
$$\boldsymbol{\nabla}\phi(f_\ell^1, y, t) \approx \epsilon \partial_y \phi^1|_0 \boldsymbol{e}_y \tag{15b}$$
$$+ \left(\partial_x \phi^0|_0 + \partial_x^2 \phi^0|_0 \epsilon f_\ell^1 + \epsilon \partial_x \phi^1|_0 \right) \boldsymbol{e}_x.$$

Similar expressions apply for $c_\pm$ and at the upper electrode. Evaluating the reaction rate at the lower electrode and expanding to first order, we find

$$R_\ell \approx R_\ell^0 + R_\ell^1, \tag{16a}$$

$$\frac{R_\ell^0}{K_0} = c_+^0 e^{\alpha Z(\phi^0 + V_\ell)} - e^{-(1-\alpha)Z(\phi^0 + V_\ell)}, \tag{16b}$$

$$\frac{R_\ell^1}{K_0} = e^{\alpha Z(\phi^0 + V_\ell)} \Big[c_+^1 + \partial_x c^0 f_\ell^1 \tag{16c}$$

$$+ c_+^0 \Big(-\bar\gamma \partial_y^2 f_\ell^1 + \alpha Z \big[\phi^1 + \partial_x \phi^0 f_\ell^1 \big] \Big) \Big]$$

$$- e^{-(1-\alpha)Z(\phi^0 + V_\ell)} \Big[-\bar\gamma \partial_y^2 f_\ell^1$$

$$- (1-\alpha)Z \big[\phi^1 + \partial_x \phi^0 f_\ell^1 \big] \Big],$$

where all fields are evaluated at $x = 0$. Similar expressions apply at the upper electrode.

Hence, the full zeroth-order problem becomes

$$0 = -\partial_x J_\pm^0, \tag{17a}$$

$$2J_\pm^0 = -\partial_x c_\pm^0 \mp Z c_\pm^0 \partial_x \phi^0, \tag{17b}$$

$$2\bar\lambda_D^2 \partial_x^2 \phi^0 = -Z(c_+^0 - c_-^0) = -\rho^0, \tag{17c}$$

with the following boundary conditions and constraints

$$J_-^0(0) = 0, \qquad J_-^0(2) = 0, \tag{18a}$$

$$J_+^0(0) = -R_\ell^0, \qquad J_+^0(2) = R_u^0, \tag{18b}$$

$$\int_0^2 \big(c_-^0 - 1 \big) \, dx = 0, \qquad \partial_x c_+^0(2) = 0, \tag{18c}$$

and the mean growth velocity U derived from Eq. (11),

$$U = a^3 c_0 J_+^0. \tag{19}$$

Similarly, the first-order problem is given by

$$\frac{D_+}{D_\pm} \partial_t c_\pm^1 = -\boldsymbol{\nabla} \cdot \boldsymbol{J}_\pm^1, \tag{20a}$$

$$2\boldsymbol{J}_\pm^1 = -\boldsymbol{\nabla} c_\pm^1 \mp Z c_\pm^0 \boldsymbol{\nabla} \phi^1 \mp Z c_\pm^1 \boldsymbol{\nabla} \phi^0, \tag{20b}$$

$$2\bar\lambda_D^2 \nabla^2 \phi^1 = -Z(c_+^1 - Z c_-^1), \tag{20c}$$

and the boundary conditions,

$$\boldsymbol{e}_x \cdot \boldsymbol{J}_-^1(2) = 0, \qquad \boldsymbol{e}_x \cdot \boldsymbol{J}_-^1(0) = 0, \tag{21a}$$

$$\boldsymbol{e}_x \cdot \boldsymbol{J}_+^1(2) = R_u^1, \qquad \boldsymbol{e}_x \cdot \boldsymbol{J}_+^1(0) = -R_\ell^1, \tag{21b}$$

$$\partial_x^2 c_+^0(2) f_u^1 + \partial_x c_+^1(2) = 0, \tag{21c}$$

together with the first-order electrode growth rates $\partial_t f_\ell^1$ and $\partial_t f_u^1$ derived from Eq. (11),

$$\partial_t f_\ell^1 = a^3 c_0 R_\ell^1, \qquad \partial_t f_u^1 = -a^3 c_0 R_u^1. \tag{22}$$

To find the eigenmodes, we make the following harmonic ansatz for the first-order fields,

$$c_\pm^1(x, y, t) = c_\pm^*(x) e^{\Gamma t + iky}, \tag{23a}$$

$$\phi^1(x, y, t) = \phi^*(x) e^{\Gamma t + iky}, \tag{23b}$$

$$f_p^1(y, t) = F_p e^{\Gamma t + iky}, \tag{23c}$$

where Γ is the nondimensional growth rate of the perturbation, and k is the wavenumber of the transverse eigenmode. For convenience we also define

$$R_p^1 = R_p^* e^{\Gamma t + iky}. \tag{23d}$$

With this ansatz, the first-order bulk equations become

$$2\frac{D_+}{D_\pm} \Gamma c_\pm^* = -k^2 (c_\pm^* \pm Z c_\pm^0 \phi^*) \tag{24a}$$

$$+ \partial_x \Big\{ \partial_x c_\pm^* \pm Z c_\pm^* \partial_x \phi^0 \pm Z c_\pm^0 \partial_x \phi^* \Big\}$$

$$2\bar\lambda_D^2 (\partial_x^2 \phi^* - k^2 \phi^*) = -Z(c_+^* - c_-^*), \tag{24b}$$

and the first-order reaction rate at the lower electrode is

$$\frac{R_\ell^*}{K_0} = e^{\alpha Z(\phi^0 + V_\ell)} \Big[c_+^* + \partial_x c^0 F_\ell$$

$$+ c_+^0 \Big(-\bar\gamma k^2 F_\ell + \alpha Z \big[\phi^* + \partial_x \phi^0 F_\ell \big] \Big) \Big]$$

$$- e^{-(1-\alpha)Z(\phi^0 + V_\ell)} \Big[-\bar\gamma k^2 F_\ell$$

$$- (1-\alpha)Z \big[\phi^* + \partial_x \phi^0 F_\ell \big] \Big]. \tag{25}$$

Inserting the ansatz in the growth equations (22) yields

$$\Gamma F_\ell = a^3 c_0 R_\ell^*, \qquad \Gamma F_u = -a^3 c_0 R_u^*. \tag{26}$$

V. ANALYTICAL RESULTS

For large wavenumbers, $k \gtrsim 1$, we can neglect f_ℓ and the left hand side in Eq. (24a). Analytical expressions for the growth rate can then be obtained in the limit of overlimiting and underlimiting current, respectively. In Appendices A and B we find that the growth rate can be expressed as

$$\Gamma = a^3 c_0 k J^0 \frac{\xi - \bar\gamma k^2}{\xi + k}. \tag{27}$$

With the usual assumption $\alpha = \frac{1}{2}$, simple expressions for ξ can be obtained. In the limit of underlimiting current $J^0 < 1$ it becomes

$$\xi = \frac{J^0}{1 - J^0} \left[\frac{1}{2} + \sqrt{1 + 4\left(\frac{K_0}{J^0}\right)^2 (1 - J^0)} \right]. \tag{28}$$

We note that the underlimiting expression is nearly identical to the one already derived by Sundstrom and Bark [16]. In the limit of overlimiting current $J^0 > 1$, we obtain

$$\xi = \frac{J^0}{c_+^0} \sqrt{1 + 4\left(\frac{K_0}{J^0}\right)^2 c_+^0}, \tag{29a}$$

$$c_+^0 \approx \frac{\bar\lambda_D}{Z} \sqrt{\frac{2J^0}{1 - \frac{1}{J^0}}}. \tag{29b}$$

The critical wavenumber k_c, where the perturbation is marginally stable, is found to be

$$k_c = \sqrt{\frac{\xi}{\bar{\gamma}}}, \tag{30a}$$

and the wavenumber k_{max}, at which the growth rate is maximum, is given as

$$k_{max} = \frac{\xi}{2}\left[\left(\frac{2 - \xi\bar{\gamma} + 2\sqrt{1 - \xi\bar{\gamma}}}{\xi\bar{\gamma}}\right)^{1/3} + \left(\frac{2 - \xi\bar{\gamma} + 2\sqrt{1 - \xi\bar{\gamma}}}{\xi\bar{\gamma}}\right)^{-1/3} - 1\right]. \tag{30b}$$

We note that the analytical model takes the zeroth-order current density J^0 as input variable through ξ. If one wants the results as a function of the potential drop instead, a model of the system's current-voltage characteristic is needed. For simplicity, we just use the numerically calculated current-voltage characteristic in the following.

To compute the results without reference to a numerical solution, an analytical model for the system's current-voltage characteristic is required. Such a model can be found in our previous work [15]. To obtain the total voltage drop over the system, the interfacial voltages from Eq. (16b) should also be taken into account.

VI. NUMERICAL SOLUTION

The numerical simulations are carried out in the commercially available finite element software COMSOL MULTIPHYSICS ver. 4.3a. Following our previous work [15, 17, 20], the zeroth- and first-order problems are rewritten in weak form and implemented in the mathematics module of COMSOL. In the first-order problem we set the parameter f_u to unity, meaning that the magnitude of the remaining first-order fields are given relative to the amplitude of the upper electrode perturbation. To limit the parameter space, we choose fixed,

TABLE I. Fixed parameter values used in the numerics.

Parameter	Symbol	Value
Cation diffusivity[18]	D_+	$0.714 \times 10^{-9}\,\mathrm{m^2\,s^{-1}}$
Anion diffusivity[18]	D_-	$1.065 \times 10^{-9}\,\mathrm{m^2\,s^{-1}}$
Ion valence	Z	2
Surface energy	γ	$1.85\ \mathrm{J\,m^{-2}}$
Temperature	T	300 K
Permittivity of water	ϵ_w	$6.90 \times 10^{-10}\,\mathrm{F\,m^{-1}}$
Charge-transfer coefficient	α	$\frac{1}{2}$
Reaction constant[a]	k_0	$9.4 \times 10^{19}\,\mathrm{m^{-2}\,s^{-1}}$
Diameter of a copper atom[b]	a	0.228 nm

[a] Calculated using the exchange current $I_0 = 30\ \mathrm{A\,m^{-2}}$ from Ref. [19] and $k_0 = I_0/(Ze)$.
[b] The cube root of the volume per atom in solid copper [18].
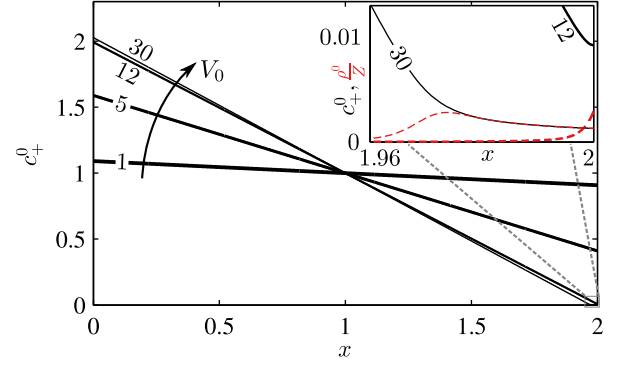

FIG. 2. (Color online) Zeroth-order cation concentrations c_+^0 shown in full (black) lines and zeroth-order charge densities ρ^0/Z shown in dashed (red) lines. The inset shows the fields close to the electrode. In the simulation the parameter values $c_0 = 10$ mM, $L = 10$ µm, and $V_0 = \{1, 5, 12, 30\}$ were used.

physically reasonable values for the parameters listed in Table I. The values are chosen to correspond to copper electrodes in a copper sulfate solution. We note that the surface tension is quite difficult to determine experimentally, and most measurements are carried out at temperatures around 1000 °C [21, 22]. *Ab initio* calculations can give some impression of the behaviour at lower temperatures [23], but these can hardly stand alone. Extrapolating the linear fit of Ref. [21] down to 0 K yields surface tension values close to those obtained from *ab initio* calculations in Ref. [23]. This makes it somewhat plausible to apply the model from Ref. [21] in the region of interest around 300 K. This yields a copper-gas surface energy of 1.92 J/m². The contact angle at the copper-water interface is very small [24], so finding the copper-water surface energy is just a matter of subtracting the surface energy of water from that of copper. The resulting surface energy is $\gamma \approx 1.85$ J/m², as listed in Table I. A great deal of uncertainty is also associated with the value of k_0, and the value of $\alpha = \frac{1}{2}$ is largely a matter of convention.

These choices leave us with three free parameters, which are the bias voltage V_0, the electrolyte concentration c_0, and the system length L.

The solution procedure is as follows: First, the zeroth-order problem is solved for a given set of parameters. Then the first-order problem is solved for a range of wavenumbers k. For each k value, the corresponding growth rate Γ and perturbation amplitude of the lower electrode, F_ℓ, are obtained.

In Fig. 2, the zeroth-order cation concentrations c_+^0 and space-charge density ρ^0 are shown for $c_0 = 10$ mM, $L = 10$ µm and varying bias voltage V_0. It is seen, that when the bias voltage exceeds $V_0 \simeq 12$, local electroneutrality is violated near the cathode. For $V_0 = 30$ the nonequilibrium space-charge region extends far ($0.04L$) into the electrolyte.
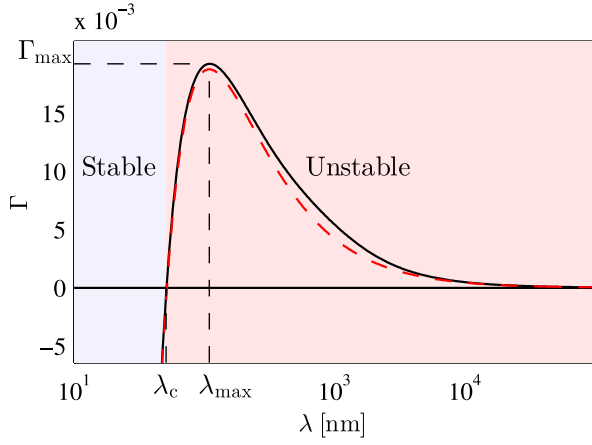
FIG. 3. (Color online) The growth rate Γ plotted versus the perturbation wavelength λ for $V_0 = 30$, $c_0 = 10$ mM, and $L = 10$ µm. The full (black) line shows the growth rate obtained from numerical simulations, and the dashed (red) line shows the growth rate according to the analytical model Eq. (27). For perturbation wavelengths smaller than the critical wavelength $\lambda_c = 51$ nm the system is stable and for larger wavelengths it is unstable. At the most unstable wavelength $\lambda_{max} = 110$ nm the growth rate is $\Gamma_{max} = 0.0193$.

A. Results

For plotting purposes we introduce the dimension-full perturbation wavelength $\lambda = 2\pi L/k$. In Fig. 3, the growth rate Γ is plotted versus λ for $V_0 = 30$, $c_0 = 10$ mM, and $L = 10$ µm. Visible in the figure is a stable region for wavelengths smaller than the critical wavelength $\lambda_c = 51$ nm, and an unstable region for larger wavelengths. The most unstable wavelength we denote λ_{max}, and the corresponding growth rate we denote Γ_{max}.

To enable a more compact representation of the data, we introduce a gray-scale contour plot of the magnitude of Γ, as illustrated in Fig. 4. Here, Γ is plotted versus the wavelength λ for $V_0 = \{5, 10, 15, 20, 25, 30\}$. The gray scale in the λ-V_0 plane is created by projecting the Γ values from the above curves onto the plane. The solid (blue) line in the (λ, V_0)-plane marks the crest of the hill, thus representing the most unstable wavelength for each value of V_0.

In Fig. 5, we make use of the contour plots to show results for twelve sets of (c_0, L)-values. In each contour plot, Γ is normalized by its maximum value, which is given above each plot. Shown in thick lines are λ_{max} in bright (yellow) and λ_c in black. The corresponding analytical results are shown in dashed (blue) and dotted (green) lines, respectively. The thin black lines show contours, where Γ equals $\{0.01, 0.2, 0.7\}$ times the maximum value. There is a clear tendency in all of the panels that the growth rate Γ increases rapidly with V_0, and the most unstable wavelength decreases as V_0 increases. Across the panels, the maximum growth rate is seen to increase for increasing c_0 and increasing L. Also, the most unstable
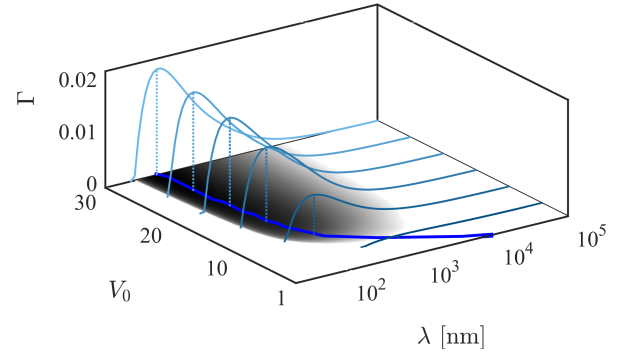

FIG. 4. (Color online) The growth rate Γ plotted versus the perturbation wavelength λ and voltage V_0 for $c_0 = 10$ mM, and $L = 10$ µm. The (cyan) space curves are plots of Γ versus λ for $V_0 = \{5, 10, 15, 20, 25, 30\}$. The shade of the in plane contour plot is based on the logarithm of Γ, which is why there are no contours in the low λ limit where Γ is negative. The thick (blue) in plane line marks the crest of the hill, i.e. it marks the most unstable wavelength for each value of V_0.

wavelength λ_{max} and the critical wavelength λ_c become smaller as c_0 increases and as L decreases.

A common feature seen in all of the panels, is the kink in the V_0-versus-λ_{max} and V_0-versus-λ_c lines. At this kink, the slope of the lines changes markedly. The kink is located at the voltage, where the current reaches the limiting current, and it thus signifies that there is a qualitatively different behavior for over- and underlimiting current. This qualitative difference between the two regimes is in accordance with the analytical models. We also see that the kink voltage changes with c_0 and L. Specifically, it increases with c_0 and decreases with L. The main reason for this behavior is easily understood with reference to the zeroth-order Butler-Volmer reaction expression (16b). Setting the current in the system to the limiting current $J_+^0 = 1$, the reaction rates at the electrodes become

$$\boldsymbol{e}_x \cdot \boldsymbol{n}_p = -K_0 \left[c_+ e^{\alpha Z(\phi + V_p)} - e^{-(1-\alpha)Z(\phi + V_p)} \right]. \quad (31)$$

At the cathode, the first term in the bracket dominates, and at the anode the other. Therefore, both potential drops over the electrode interfaces scale as

$$\Delta V \sim -\ln(K_0) = \ln\left(\frac{2D_+ c_0}{L}\right) - \ln(k_0), \quad (32)$$

which increases monotonically with increasing c_0/L. As a consequence, the total potential drop at the limiting current also increases with increasing c_0/L, just as observed in Fig. 5.

In addition to the instability growth rate Γ, which gives a time scale for the development of instabilities, it is useful to have a measure for the characteristic instability length scale. For instance, we would like to estimate the thickness of the deposited layer, when instabilities start to develop. We define this instability length scale as the
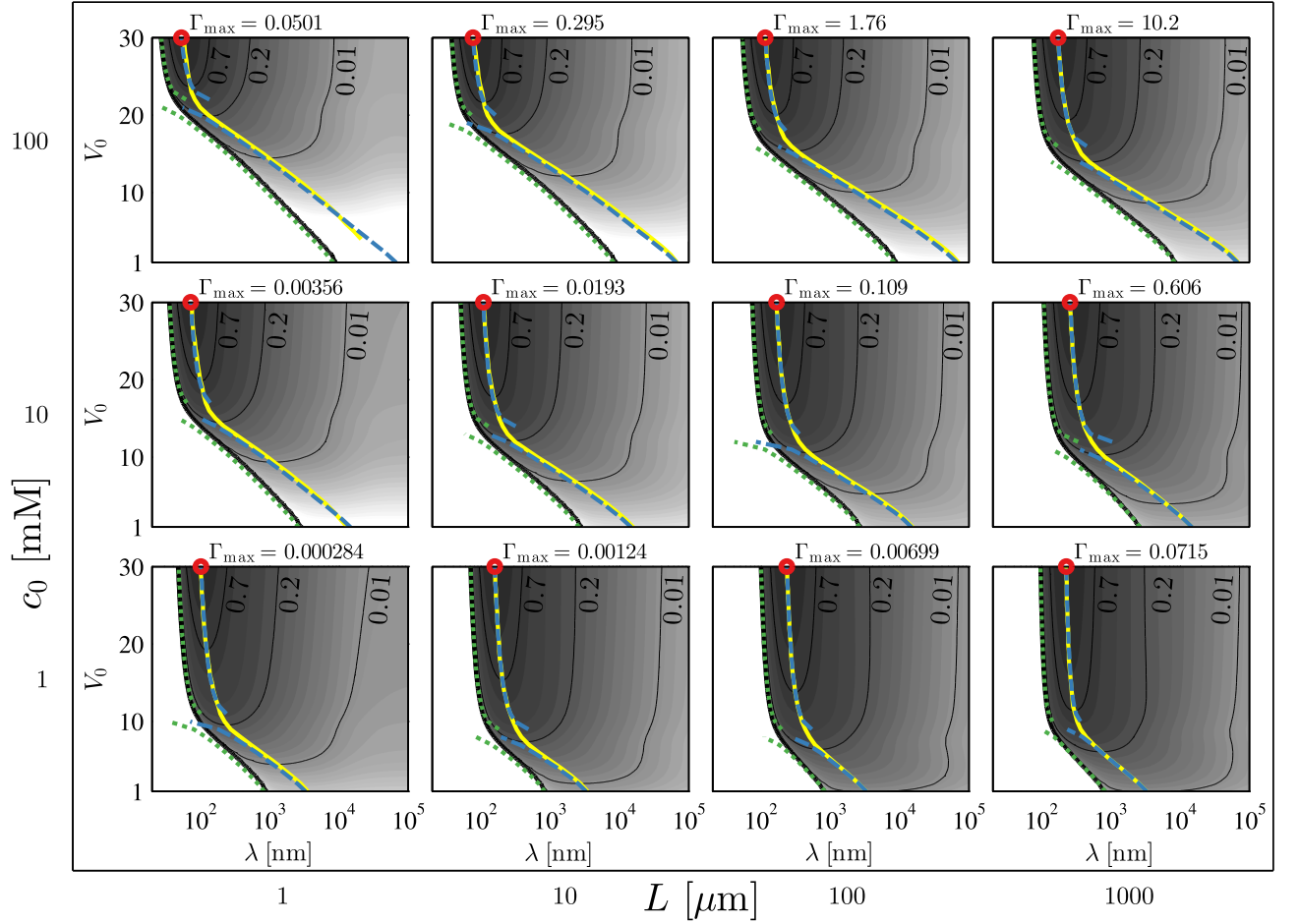
FIG. 5. (Color online) Contour plots of Γ plotted versus wavelength λ and voltage V_0 for $c_0 = \{1\text{ mM}, 10\text{ mM}, 100\text{ mM}\}$ and $L = \{1\text{ μm}, 10\text{ μm}, 100\text{ μm}, 1\text{ mm}\}$. In each plot, Γ is normalized by its maximum value, and the contours are logarithmically spaced. The maximum value Γ_{max} of Γ is given on top of each plot, and the point where the maximum value is attained is indicated with a dark (red) circle. The three thin black lines in each plot indicate contours where Γ equals 0.01, 0.2, and 0.7 times Γ_{max}. The thick bright (yellow) line marks λ_{max} for each value of V_0, and the dashed (blue) lines mark the two corresponding analytical limits. The thick black line marks λ_c for each value of V_0, and the dotted (green) lines mark the two corresponding analytical limits.

product of the zeroth-order growth rate Eq. (19) and the instability time scale at the most unstable wavelength

$$L_\Gamma = L \frac{a^3 c_0 J_+^0}{\Gamma_{\text{max}}}, \qquad (33)$$

where the pre-factor L ensures a dimensionfull expression. In Fig. 6, we plot the instability length L_Γ versus applied voltage V_0 for $L = 100$ μm and varying c_0. The most unstable wavelength λ_{max} is also plotted in the same figure (dashed lines). It is seen that L_Γ decreases as V_0 increases, but for small voltages L_Γ is largest for high concentrations, while the opposite is true for high voltages. The reason for this reversal is that the interfacial voltage drops are largest for large c_0. At small voltages the bulk driving force in the systems with large c_0 is therefore small, and this causes the system to be less unstable than the low c_0 systems. We also see that λ_{max} scales in the same way as L_Γ. While the reason for

this is not immediately obvious, it is seen to follow from the analytical expressions. Inserting Eq. (27) in Eq. (33) yields

$$L_\Gamma = \frac{\lambda_{\text{max}}}{2\pi} \frac{\xi + \frac{2\pi L}{\lambda_{\text{max}}}}{\xi - \bar{\gamma}\left(\frac{2\pi L}{\lambda_{\text{max}}}\right)^2}, \qquad (34)$$

which confirms the approximate scaling between L_Γ and λ_{max}. The connection between L_Γ and λ_{max} implies that λ_{max} sets the scale, not only for the variations in the horizontal direction, but also for variations in the vertical direction. We might therefore expect that the ramified electrodeposits, emerging at much longer times than Γ_{max}^{-1}, have a universal length scale roughly set by λ_{max}.
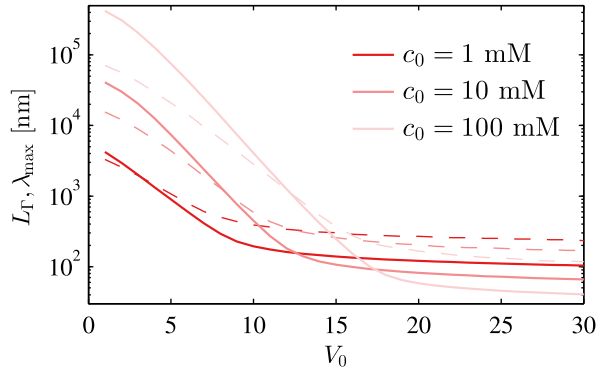
FIG. 6. (Color online) The instability length scale L_Γ (full line) and most unstable wavelength $\lambda_{\max}$ (dashed line) plotted versus bias voltage V_0. The concentration varies between the values $c_0 = \{1\text{ mM}, 10\text{ mM}, 100\text{ mM}\}$ and the length $L = 100$ μm was used.

VII. DISCUSSION

The main feature, which sets our work apart from previous stability analyses of electrodeposition, is the inclusion of the overlimiting regime. Presumably, this regime has so far been avoided due to the non-linearities arising at overlimiting current, which necessitate a more complicated treatment. However, the overlimiting regime is highly relevant for ramified growth problems [7, 8]. As seen in Fig. 5, the instability growth rate increases markedly in the overlimiting regime, and there is also a change in qualitative behavior between the two regimes. Of course, the conclusions we reach, based on our model, are only strictly valid for planar electrodes. It does, however, seem reasonable to expect that the most unstable wavelength $\lambda_{\max}$ is comparable to the characteristic dimensions encountered in a ramified growth experiment. Our analysis can thus be used to rationalize experimental results. In this regard, our analytical models are particularly useful, since they allow for easy computation of the key parameters for other systems than the one treated here.

Perhaps the most important application of the stability analysis, is as a means of validating more elaborate numerical models of ramified growth. A model of ramified growth must necessarily deal with a moving interface and this, as well as other complications, make for highly complex numerical models. To validate such models it is very useful to have a comparatively simple model, like the present one, to benchmark against in the relevant limit. Indeed, this was what originally motivated us to treat the stability problem.

An obvious shortcoming of the given analysis, is the restriction to a steady-state zeroth-order solution. The principal reason for this choice is that it makes for a simpler problem. Furthermore, the numerical ramified growth model, to which we wish to compare our model, is at present also restricted to quasi-steady state. In time,

we wish to extend both models to the fully transient regime.

There is, however, some physical justification for making the steady-state assumption. As seen in Fig. 5, the growth rate Γ is considerably smaller than unity in a large part of the investigated parameter space. The time it takes the system to reach steady state is given by the diffusive time, which in our normalization has the value one. Thus, as long as Γ is much smaller than unity, the system reaches steady state long before any instabilities build up. In this case it is therefore justified to assume steady state. It should be noted that in this argument we make the reasonable assumption that the true growth rate in the transient regime does not significantly exceed the steady-state value.

To model the reaction rate at the electrodes we use the standard Butler-Volmer expression, which stands at the core of much electrochemistry. The Butler-Volmer model is, however, largely a phenomenological model, that does not necessarily apply in all regimes [25]. As applied here, the model does not distinguish between the potential drop over the Debye layer and the potential drop in the narrow interface region. This does not seem quite right, but it could be fixed with relative ease by implementing the Frumkin correction to the Butler-Volmer model. Nevertheless, to be in accordance with most previous studies, and because the Frumkin correction would introduce another unknown parameter, we have chosen not to make this correction.

VIII. CONCLUSION

We have successfully solved the stability problem in the under- and overlimiting regime for the case of a copper sulfate solution trapped between two copper electrodes. In addition to the numerical solution of this particular problem, we have derived analytical solutions valid in either the overlimiting or the underlimiting limit. The behavior in the overlimiting regime differs qualitatively from the behavior in the underlimiting regime, and we find that the electrode becomes increasingly unstable as the current is increased above the limiting current. The stability analysis, and in particular the analytical limits, are valuable both for rationalizing experimental results and for validating more elaborate numerical models of ramified growth.

Appendix A: The electroneutral limit

In the limit where the electrolyte is locally electroneutral and the time derivatives in the first-order transport problem are negligible, analytical solutions to the problem can be obtained. Setting the point of zero electrostatic potential at $x = 1$, it is easily found that

$$c = c_+ = c_- = e^{Z\phi}. \tag{A1}$$

It follows that $c = e^{Z(\phi^0 + \phi^1)} \approx e^{Z\phi^0} + e^{Z\phi^0} Z\phi^1$, and thus

$$c^0 = e^{Z\phi^0} \quad \text{and} \quad c^1 = e^{Z\phi^0} Z\phi^1. \quad \text{(A2)}$$

Solving the zeroth-order problem yields

$$c^0 = 1 - J^0(x-1), \quad Z\phi^0 = \ln(1 - J^0(x-1)). \quad \text{(A3)}$$

Using the electroneutrality assumption in Eq. (24a) we find

$$0 = \partial_x^2 c^* - k^2 c^*. \quad \text{(A4)}$$

This equation has two solutions, but as long as the perturbation wavelength is considerably smaller than the electrode spacing, the solution which increases with x is dominant

$$c^* \approx C e^{k(x-2)}, \quad \text{(A5)}$$

where C is a constant to be determined. From Eq. (A2) we then find

$$\phi^* = \frac{1}{Z} \frac{c^*}{c^0} = \frac{C}{Z} \frac{e^{k(x-2)}}{1 - J^0(x-1)}. \quad \text{(A6)}$$

At the upper electrode, $x = 2$, the first-order reaction rate is (we set $F_u = 1$)

$$\frac{R_u^*}{K_0} =$$
$$e^{\alpha Z(\phi^0 + V_u)}\left[c^* + \partial_x c^0 + c_+^0\left(\bar{\gamma}k^2 + \alpha Z[\phi^* + \partial_x \phi^0]\right)\right]$$
$$- e^{-(1-\alpha)Z(\phi^0 + V_u)}\left[\bar{\gamma}k^2 - (1-\alpha)Z[\phi^* + \partial_x \phi^0]\right]. \quad \text{(A7)}$$

We can simplify this expression by using

$$e^{-(1-\alpha)Z(\phi^0 + V_u)} = c^0 e^{\alpha Z(\phi^0 + V_u)} - \frac{R_u^0}{K_0}, \quad \text{(A8)}$$

from the zeroth-order reaction expression. The first-order reaction expression then becomes

$$\frac{R_u^*}{K_0} = e^{\alpha Z(\phi^0 + V_u)}\left[c^* + \partial_x c^0 + c_+^0 Z\left(\phi^* + \partial_x \phi^0\right)\right]$$
$$+ \frac{R_u^0}{K_0}\left[\bar{\gamma}k^2 - (1-\alpha)Z\left(\phi^* + \partial_x \phi^0\right)\right]. \quad \text{(A9)}$$

Evaluating the fields at $x = 2$, this expression becomes

$$\frac{R_u^*}{K_0} = 2(C - J^0)e^{\alpha Z(\phi^0 + V_u)}$$
$$+ \frac{J^0}{K_0}\left[\bar{\gamma}k^2 - (1-\alpha)\frac{C - J^0}{1 - J^0}\right]. \quad \text{(A10)}$$

The current into the upper electrode is $J^* = -\partial_x c^* = -kC$, meaning that

$$-kC = R_u^* = 2(C - J^0)K_0 e^{\alpha Z(\phi^0 + V_u)}$$
$$+ J^0 \bar{\gamma}k^2 - (1-\alpha)J_0 \frac{C - J^0}{1 - J^0}, \quad \text{(A11)}$$

and solving for C, we obtain

$$C = J^0 \frac{-2K_0 e^{\alpha Z(\phi^0 + V_u)} + \bar{\gamma}k^2 + (1-\alpha)\frac{J^0}{1-J^0}}{-2K_0 e^{\alpha Z(\phi^0 + V_u)} - k + (1-\alpha)\frac{J^0}{1-J^0}}. \quad \text{(A12)}$$

The growth rate can be expressed as

$$\Gamma = -a^3 c_0 J^* = a^3 c_0 kC, \quad \text{(A13)}$$

so we have

$$\Gamma = a^3 c_0 k J^0 \frac{2K_0 e^{\alpha Z(\phi^0 + V_u)} - \bar{\gamma}k^2 - (1-\alpha)\frac{J^0}{1-J^0}}{2K_0 e^{\alpha Z(\phi^0 + V_u)} + k - (1-\alpha)\frac{J^0}{1-J^0}} \quad \text{(A14)}$$

For the special case where $\alpha = \frac{1}{2}$ we find from the zeroth-order current that

$$2K_0 e^{\alpha Z(\phi^0 + V_u)} = \frac{J^0}{c^0}\left[1 + \sqrt{1 + 4\left(\frac{K_0}{J^0}\right)^2 c^0}\right]. \quad \text{(A15)}$$

Inserting this yields

$$\Gamma = a^3 c_0 k J^0 \frac{\frac{J^0}{1-J^0}\left[\alpha + \sqrt{1 + 4\left(\frac{K_0}{J^0}\right)^2 (1-J^0)}\right] - \bar{\gamma}k^2}{\frac{J^0}{1-J^0}\left[\alpha + \sqrt{1 + 4\left(\frac{K_0}{J^0}\right)^2 (1-J^0)}\right] + k}, \quad \text{(A16)}$$

an expression which accurately replicates the numerical results at low voltages and low $\bar{\lambda}_D$.

To test whether the time derivatives in the first-order problem really are negligible, we compare the time derivative term $2\Gamma c_+^*$ with the transverse diffusion term $k^2 c_+^*$. Since Eq. (A16) implies $\Gamma \leq a^3 c_0 k J^0$, our assumption is justified if

$$2a^3 c_0 J^0 \ll k. \quad \text{(A17)}$$

Consequently, because $a^3 c_0 \ll 1$ for dilute systems and J^0 is of order unity, it is justified to neglect the time derivative, unless the perturbation wavelength is much larger than the electrode spacing.

The critical wavenumber k_c is found by setting the nominator in Eq. (A16) equal to zero,

$$k_c = \sqrt{\frac{\xi}{\bar{\gamma}}}, \quad \text{(A18)}$$

where we have introduced the parameter

$$\xi = \frac{J^0}{1 - J^0}\left[\alpha + \sqrt{1 + 4\left(\frac{K_0}{J^0}\right)^2 (1 - J^0)}\right]. \quad \text{(A19)}$$

To find the wavenumber $k_{\max}$, at which Γ attains its maximum $\Gamma_{\max}$, we set the derivative of Γ equal to zero and

solve for k,

$$k_{\max} = \frac{\xi}{2}\left[\left(\frac{2 - \xi\bar{\gamma} + 2\sqrt{1 - \xi\bar{\gamma}}}{\xi\bar{\gamma}}\right)^{1/3}\right.$$
$$\left. + \left(\frac{2 - \xi\bar{\gamma} + 2\sqrt{1 - \xi\bar{\gamma}}}{\xi\bar{\gamma}}\right)^{-1/3} - 1\right], \quad \text{(A20)}$$

with the asymptotic solutions,

$$k_{\max} \approx \begin{cases} \left(\frac{\xi}{3\bar{\gamma}}\right)^{1/2}, & \text{for } \bar{\gamma}\xi \gg 1, \\ \left(\frac{\xi^2}{2\bar{\gamma}}\right)^{1/3} - \frac{\xi}{2}, & \text{for } \bar{\gamma}\xi \ll 1. \end{cases} \quad \text{(A21)}$$

Appendix B: The strongly non-linear limit

In the limit where the driving force is very large, some of the terms in Eqs. (24a) and (24b) become dominant, which makes an analytical solution of the problem possible.

If the system is strongly driven, the field gradients are large close to the upper electrode, and this makes the electrode surface much more unstable. It follows that a larger k value is needed for the surface tension to stabilize the system, so the most unstable value of k will be larger than for less driven systems. In the strongly driven limit, we might therefore expect that Eq. (24b) largely is a balance between $\partial_x^2\phi^*$ and $k^2\phi^*$ in the region of interest. This leads us to making the ansatz

$$\phi^* = \Phi e^{k(x-2)}, \quad \text{(B1)}$$

where Φ is a constant. We now consider Eq. (24a) for the cation concentration, neglecting the left hand side

$$0 = -\partial_x\left\{-\partial_x c_+^* - Zc_+^*\partial_x\phi^0 - Zc_+^0\partial_x\phi^*\right\}$$
$$- k^2(c_+^* + Zc_+^0\phi^*). \quad \text{(B2)}$$

We assume that the terms $\partial_x c_+^*$ and $Zc_+^*\partial_x\phi^0$ are negligible compared to $Zc_+^0\partial_x\phi^*$ and insert the ansatz Eq. (B1)

$$0 \approx Z\partial_x c_+^0 k\phi^* + Zc_+^0 k^2\phi^* - k^2(c_+^* + Zc_+^0\phi^*) \quad \text{(B3)}$$
$$\approx Z\partial_x c_+^0 k\phi^* - k^2 c_+^*, \quad \text{(B4)}$$

implying that

$$c_+^* \approx \frac{Z}{k}\partial_x c_+^0 \phi^*. \quad \text{(B5)}$$

To test the assumptions leading to this result, we need expressions for c_+^0, $\partial_x c_+^0$ and $\partial_x\phi^0$. From Ref. [15] we have such expressions, and in the extended space-charge region (ESC) they take the simple forms

$$c_+^0(x) \approx \sqrt{2}\frac{\bar{\lambda}_{\rm D}}{Z}\sqrt{J^0}\left[x - 1 - \frac{1}{J^0}\right]^{-1/2}, \quad \text{(B6)}$$

$$\partial_x c_+^0(x) \approx -\frac{\sqrt{2}}{2}\frac{\bar{\lambda}_{\rm D}}{Z}\sqrt{J^0}\left[x - 1 - \frac{1}{J^0}\right]^{-3/2}, \quad \text{(B7)}$$

$$\partial_x\phi^0(x) \approx -\frac{\sqrt{2}}{\bar{\lambda}_{\rm D}}\sqrt{J^0}\left[x - 1 - \frac{1}{J^0}\right]^{1/2}. \quad \text{(B8)}$$

The width of the ESC is given as $L_{\rm ESC} = 1 - 1/J^0$, so in the region close to the electrode, compared to the width of the ESC, the fields can be written as

$$c_+^0(x) \approx \sqrt{2}\frac{\bar{\lambda}_{\rm D}}{Z}\sqrt{J^0}L_{\rm ESC}^{-1/2}, \quad \text{(B9)}$$

$$\partial_x c_+^0(x) \approx -\frac{c_+^0}{2L_{\rm ESC}}, \quad \text{(B10)}$$

$$\partial_x\phi^0(x) \approx -\frac{Zc_+^0}{\bar{\lambda}_{\rm D}^2}L_{\rm ESC}. \quad \text{(B11)}$$

Evaluating $\partial_x c_+^*$ we find

$$\partial_x c_+^* \approx \frac{Z}{k}\frac{3c_+^0}{4L_{\rm ESC}^2}\phi^* - Z\frac{c_+^0}{2L_{\rm ESC}}\phi^*, \quad \text{(B12)}$$

which is seen to be much smaller than $Zc_+^0\partial_x\phi^*$ if

$$2k \gg \frac{1}{L_{\rm ESC}}, \quad \text{(B13)}$$

that is, if the perturbation wavelength satisfies

$$\bar{\lambda} \ll 4\pi L_{\rm ESC}. \quad \text{(B14)}$$

Similarly, we find that $Zc_+^*\partial_x\phi^0$ is much smaller than $Zc_+^0\partial_x\phi^*$ if

$$\bar{\lambda}^2 \ll \frac{8\pi^2}{Z^2}\frac{\bar{\lambda}_{\rm D}^2}{c_+^0(2)}. \quad \text{(B15)}$$

Finally, the ansatz Eq. (B1) is justified if $2\bar{\lambda}_{\rm D}^2 k^2\phi^* \gg Zc_+^*$, which is equivalent to

$$\bar{\lambda}^3 \ll \frac{32\pi^3}{Z^2}\frac{\bar{\lambda}_{\rm D}^2}{c_+^0(2)}L_{\rm ESC}. \quad \text{(B16)}$$

This last requirement is seen to follow if the two first requirements Eqs. (B14) and (B15) are fulfilled.

In the strongly driven regime, where Eqs. (B14) and (B15) are satisfied, the first-order current is approximately

$$2J_+^* \approx -Zc_+^0\partial_x\phi^* = -Zkc_+^0\Phi, \quad \text{(B17)}$$

at the upper electrode. The zeroth-order diffusive contribution is also very small at the upper electrode, meaning

that we can simplify Eq. (A9)

$$R_u^* \approx K_0 e^{\alpha Z(\phi^0 + V_u)} \left[c_+^0 Z(\phi^* + \partial_x \phi^0) \right]$$
$$+ R_u^0 \left[\bar{\gamma} k^2 - (1-\alpha) Z(\phi^* + \partial_x \phi^0) \right] \qquad \text{(B18)}$$

$$\approx K_0 e^{\alpha Z(\phi^0 + V_u)} \left[c_+^0 Z\Phi - 2J^0 \right]$$
$$+ R_u^0 \left[\bar{\gamma} k^2 - (1-\alpha)\left(Z\Phi - \frac{2J^0}{c_+^0} \right) \right]. \qquad \text{(B19)}$$

Inserting $R_u^* = J_+^* \approx -\frac{1}{2} Z k c_+^0 \Phi$ we find

$$\frac{Z}{2} k c_+^0 \Phi = k J^0 \frac{2K_0 e^{\alpha Z(\phi^0 + V_u)} - \bar{\gamma} k^2 - (1-\alpha)\frac{2J^0}{c_+^0}}{2K_0 e^{\alpha Z(\phi^0 + V_u)} + k - (1-\alpha)\frac{2J^0}{c_+^0}}, \qquad \text{(B20)}$$

and since $\Gamma = -a^3 c_0 J^*$

$$\Gamma = a^3 c_0 k J^0 \frac{2K_0 e^{\alpha Z(\phi^0 + V_u)} - \bar{\gamma} k^2 - (1-\alpha)\frac{2J^0}{c_+^0}}{2K_0 e^{\alpha Z(\phi^0 + V_u)} + k - (1-\alpha)\frac{2J^0}{c_+^0}} \qquad \text{(B21)}$$

$$= a^3 c_0 k J^0 \frac{\frac{J^0}{c_+^0}\left[2\alpha - 1 + \sqrt{1 + 4\left(\frac{K_0}{J^0}\right)^2 c_+^0} \right] - \bar{\gamma} k^2}{\frac{J^0}{c_+^0}\left[2\alpha - 1 + \sqrt{1 + 4\left(\frac{K_0}{J^0}\right)^2 c_+^0} \right] + k}, \qquad \text{(B22)}$$

where the second expression assumes $\alpha = \frac{1}{2}$, so that Eq. (A15) is valid. Like in the electroneutral limit neglecting the time derivative in the first-order problem is justified, unless the perturbation wavelength is much larger than the electrode spacing. The expressions (A18) and (A20) are also valid for the strongly nonlinear limit, if instead of Eq. (A19) we use

$$\xi = \frac{J^0}{c_+^0}\left[2\alpha - 1 + \sqrt{1 + 4\left(\frac{K_0}{J^0}\right)^2 c_+^0} \right]. \qquad \text{(B23)}$$

[1] G. Libbrecht, Rep Prog Phys **68**, 855 (2005).
[2] R. Trivedi and W. Kurz, Int Mater Rev **39**, 49 (1994).
[3] R. M. Brady and R. C. Ball, Nature **309**, 225 (1984).
[4] N. Nikolic, K. Popov, L. Pavlovic, and M. Pavlovic, Surf Coat Technol **201**, 560 (2006).
[5] G. Kahanda and M. Tomkiewicz, J electrochem soc **136**, 1497 (1989).
[6] C. Leger, J. Elezgaray, and F. Argoul, Phys Rev E **61**, 5452 (2000).
[7] G. Gonzalez, M. Rosso, and E. Chassaing, Phys Rev E **78**, 011601 (2008).
[8] J.-H. Han, E. Khoo, P. Bai, and M. Bazant, Sci. Rep. **4**, 7056 (2014).
[9] P. Trigueros, J. Claret, F. Mas, and F. Sagues, J Electroanal Chem **312**, 219 (1991).
[10] O. Devos, C. Gabrielli, L. Beitone, C. Mace, E. Ostermann, and H. Perrot, J. Electroanal. Chem **606**, 75 (2007).
[11] K. Nishikawa, E. Chassaing, and M. Rosso, J Electrochem Soc **160**, D183 (2013).
[12] J. N. Chazalviel, Phys. Rev. A **42**, 7355 (1990).
[13] M. Rosso, Electrochim. Acta **53**, 250 (2007).
[14] M. Rosso, J. N. Chazalviel, and E. Chassaing, J Electroanal Chem **587**, 323 (2006).
[15] C. P. Nielsen and H. Bruus, Phys Rev E **89**, 042405 (2014).
[16] L. Sundstrom and F. Bark, Electrochim Acta **40**, 599 (1995).
[17] C. P. Nielsen and H. Bruus, Phys Rev E **90**, 043020 (2014).
[18] D. R. Lide, *CRC Handbook of Chemistry and Physics*, 91st ed., edited by W. M. Haynes, (Internet Version 2011) (CRC Press/Taylor and Francis, Boca Raton, FL, 2010).
[19] D. R. Turner and G. R. Johnson, J Electrochem Soc **109**, 798 (1962).
[20] M. M. Gregersen, M. B. Andersen, G. Soni, C. Meinhart, and H. Bruus, Phys Rev E **79**, 066316 (2009).
[21] H. Udin, A. J. Shaler, and J. Wulff, Trans. AIME **185**, 186 (1949).
[22] V. K. Kumikov and K. B. Khokonov, J. Appl. Phys. **54**, 1346 (1983).
[23] H. L. Skriver and N. M. Rosengaard, Phys rev B **46**, 7157 (1992).
[24] D. J. Trevoy and H. Johnson, J. Phys. Chem. **62**, 833 (1958).
[25] M. Z. Bazant, Acc. Chem. Res. **46**, 1144 (2013).